

Defect-induced magnetism and Yu-Shiba-Rusinov states in twisted bilayer graphene

Alejandro Lopez-Bezanilla^{1,*} and J. L. Lado²

¹*Theoretical Division, Los Alamos National Laboratory, Los Alamos, New Mexico 87545, USA*

²*Institute for Theoretical Physics, ETH Zurich, 8093 Zurich, Switzerland*

(Dated: June 7, 2019)

Atomic defects have a significant impact in the low-energy properties of graphene systems. By means of first-principles calculations and tight-binding models we provide evidence that chemical impurities modify both the normal and the superconducting states of twisted bilayer graphene. A single hydrogen atom attached to the bilayer surface yields a triple-point crossing, whereas self-doping and three-fold symmetry-breaking are created by a vacant site. Both types of defects lead to time-reversal symmetry-breaking and the creation of local magnetic moments. Hydrogen-induced magnetism is found to exist also at the doping levels where superconductivity appears in magic angle graphene superlattices. As a result, the coexistence of superconducting order and defect-induced magnetism yields in-gap Yu-Shiba-Rusinov excitations in magic angle twisted bilayer graphene.

I. INTRODUCTION

The tunability of graphene¹ and two-dimensional materials has provided an outstanding solid-state platform to explore emergent physical phenomena. Yet, on top of its standalone interest, graphene provides a powerful building block to create superstructures due to the weak van der Waals forces between layers.² Those very same weak van der Waals forces allow to deposit graphene layers on top of each other with relative angles, in stark contrast with conventional bulk crystals. Twisted bilayer graphene (tBLG)³ is one the simplest structures that can be built in that fashion, and has opened the door towards realizing states of matter inaccessible in monolayer graphene.^{4–9} This additional flexibility stems from the emergent moiré pattern that arises due to the twist between the layers, giving rise to an emergent electronic structure that can be controlled by the twist angle.^{10–13}

A paradigmatic example of new physics associated with the emergent moiré band structure is the appearance of superconductivity in magic angle graphene ($\alpha \approx 1^\circ$) superlattices,⁵ that exploit a chemical-free field effect doping of graphene without altering its structural integrity. Moreover, experimental observations reported strong correlated behavior,⁶ anomalous Hall effect,⁷ strange metal behavior⁸, and rotational symmetry-breaking⁹ close to that regime. Extensive theoretical efforts are being directed towards deriving a faithful low-energy model,^{14–17} studying the possible electronic instabilities,^{18,19} and providing means of tailoring the electronic properties of such state.^{20–22} However, the influence of atomic defects in this structures has not been addressed in detail, and their potential impact in the low-energy properties has remained rather unexplored.^{23,24}

In this paper, we study the impact of atomic defects in tBLG with angles ranging from large angles $\alpha \approx 5^\circ$ to the magic angle $\alpha \approx 1^\circ$. First-principles methods and effective real-space tight-binding models are used to describe two paradigmatic defects in graphene systems, namely carbon vacancies^{25–29} and chemisorbed

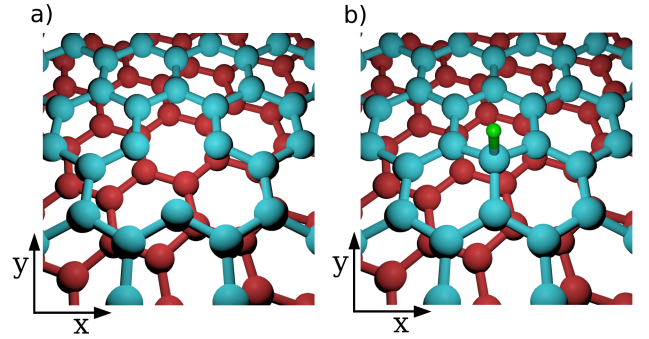


FIG. 1. Sketch of the two defects considered in tBLG, a carbon vacancy a) and a chemisorbed hydrogen atom b). Blue denotes the upper layer, red the lower layer and green the hydrogen atom. Both defect create impurity bands close the charge neutrality point that give rise to local magnetic moments, substantially impacting the low-energy properties of twisted bilayers.

H atoms^{23,24,30–32} as shown in Fig. 1. In particular, the chemical modification introduced by monohydrogenation creates flat bands at the Fermi energy, whose unbalanced electronic occupation yields local magnetic moments. In the superconducting state of magic angle tBLG, such magnetic moments are shown to in-gap Yu-Shiba-Rusinov excitations, dramatically impacting the spectral properties of the superconducting state.

The manuscript is organized as follows. In Sec. II the emergence of magnetism as a result of both C vacancies and mono-hydrogenation is analyzed with first-principles calculations. Sec. III shows that chemisorbed H can be treated with a low-energy model that reproduces accurately the first-principles results. In Sec. IV we show that the interplay between impurity induced magnetism and superconductivity gives rise to in-gap Yu-Shiba-Rusinov states. Finally, Sec. V summarizes our conclusions.

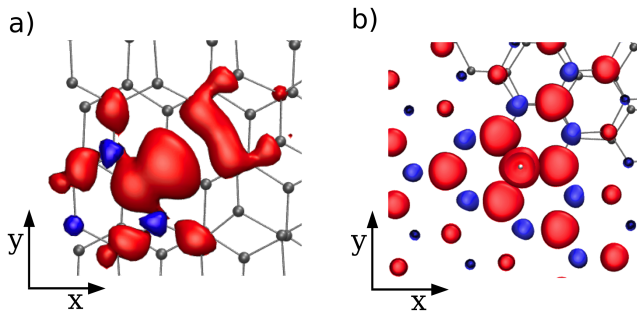


FIG. 2. Real-space redistribution of the charge density of two different defects in twisted bilayer graphene at $\alpha = 5.09^\circ$. Top view of the charge distribution of a single vacancy, a) and a single H atom, b). A single-H atom creates a triangular distribution around the defect, whilst the vacant site enhances the net charge localization at the σ dangling bonds. Isosurfaces correspond to charge densities of $10^{-3} \text{ e}^- \text{ \AA}^{-3}$ (a), b)) and $10^{-2} \text{ e}^- \text{ \AA}^{-3}$ (c))

II. DEFECT-INDUCED STATES FROM FIRST PRINCIPLES

A. General considerations

We first study the effect of structural and chemical modification of tBLG with first-principle methods. Moiré lattices are created by twisting a graphene layer over the other by a commensurate angle, so that a unit cell with coincidence site lattice points is created^{3,33,34}. In the chosen tBLG geometry, one layer of AA-bilayer graphene is rotated an angle $\theta = 5.09^\circ$ with respect to the other layer. Internal coordinates of pristine and modified tBLGs separated initially by the van der Waals distance of 3.3 \AA were fully relaxed. The momentum mismatch between the layers yields two linearly dispersive bands, which are degenerate in the $\Gamma - K - M$ high-symmetry path of the BZ.^{3,10,11,35,36}

First-principles calculations provide a powerful insight on effect of structural relaxation on the electronic structure of defective systems, together with the properties of the remaining unpaired electron. Chemisorption of a single H atom^{23,24,30–32} is a simple way of creating an imbalance between the number of A and B sites in graphene, with bare modification of the bipartite nature of graphene lattice^{37–47}. The imbalance between the number of sites in the two sublattices has an important consequence that follows from Lieb’s theorem⁴⁸: a bipartite lattice with more A sites than B sites will show a number of zero modes proportional to such difference. In a similar fashion, a vacant C site breaks the lattice symmetry by removing one atom, but creating additional distortions^{49–55}. In an oversimplified picture, both approaches are equivalent to removing a π electron. However, the sp^3 rehybridization of an atom or the creation of dangling σ -bond have completely different consequences on the localization and dispersion of the electronic state.

This feature can be clearly seen in the charge redistribution of Fig. 2, where it is shown that the vacancy triggers an atomic reconstruction that breaks C_3 symmetry (Fig. 2a), whereas the hydrogen ad-atom creates a redistribution that conserves the original three-fold rotation (Fig. 2b).

Due to the varying distance between C atoms across the parallel layers, the effect of a H atom depends on its location.^{38,56–59} Similarly, a vacant site interacts differently with the opposite graphene layer depending on the stacking region where the C atom was removed from.^{60–62} In the following, we address in detail the electronic reconstruction associated to each one of the defects introduced.

B. Carbon vacancy

Within the DFT formalism, a vacancy is more than a simple removal of a lattice site, and reconstruction of the whole tBLG structure is considered²⁵. Atomic rearrangement is present in real systems, and thus removing a C atom out of one of the graphene sheet has a non-trivial effect on the distribution of electronic states in the low-energy band diagram. Fig. 3a displays a paramagnetic calculation of a fully relaxed tBLG structure with a vacant site. The electronic state at the Fermi level corresponds to the defect state, which removes the degeneracy of the bands that form the Dirac cones and creates an almost degenerate (4 meV gaped) triple-crossing at the K point. The vacancy state creates a major disruption on one of the sets of linear bands, pushing them at higher and lower energies.

By introducing the spin degree of freedom, a magnetic ground state with an associated spin splitting of the defect band is found (Fig.3b). A magnetic moment of $1.5 \mu_B$ is created as a result of the p-type doping character that unbalances the π -bands filling at the Fermi level. A vacancy in a tBLG polarizes the bilayer by distorting the dispersion of the π -bands and introducing a p-doping on the opposite layer that unbalances the electronic population of the valence bands. Furthermore, the defect creates two spin-dependent dispersionless bands at very different energies, (-0.5 and 1.35 eV for spin- \uparrow and spin- \downarrow respectively) as show in Fig.3b, and whose spatial extension is reduced to the immediate surrounding of the vacancy. Real-space representation of the charge density distribution in Fig.2a shows that the unpaired electron is located in the σ -bonds of the C atoms at the vacant site. The highly localized nature of the defect, together with the location of its electronic states in the band diagram is expected to yield a greatly enhanced signal in a scanning tunnel microscope experiment.^{23,25}

Removing one electron out of the system barely changes the shape of the electronic bands, but empties completely the spin- \uparrow band, leaving the other partially filled (see Fig.3c). A total magnetic moment of $0.9 \mu_B$ is obtained, similarly to the case of monolayer graphene²⁵. Removing an additional C atom near to the removed site

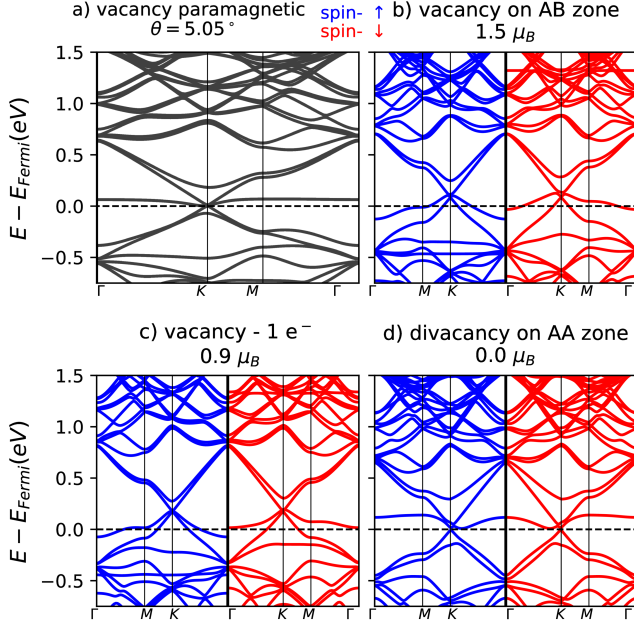


FIG. 3. a) First-principles paramagnetic electronic band structure of a bilayer graphene with a twist angle of $\alpha = 5.09^\circ$ and a C atom vacancy. Spin-polarized calculations yield a spin splitting of the defect-induced band. In b), a vacancy in the AB stacking zone yields a magnetic moment of $1.5 \mu_B$, which is lowered to $0.9 \mu_B$ when removing one electron. A divacancy exhibits a paramagnetic configuration and an empty nearly flat-state at Fermi level. In all four cases the impurity state exhibits at Γ point an energy in between the two Dirac cones.

creates a divacancy, that restores the non-magnetic state of the structure by effectively removing the unpaired electrons of the single-vacancy. As shown in Fig. 3d, a defect state similar to the paramagnetic single vacancy state is located in the vicinity of the Fermi level and the flat bands at low and high energies disappear.

C. Chemisorbed hydrogen atom

We now move on to consider the effect of a single H atom attached to one of the graphene layers. Relaxation of the entire structure results on the adsorbent C atom site pulled out of the graphene plane, adopting the pyramidal geometry characteristic of the sp^3 hybridization. Moreover, the bond lengths between the anchoring carbon atom and its first neighboring atoms were elongated to 1.49 Å, and the C-H bonding distance is of 1.14 Å. Interestingly, the atomic reconstruction preserves the local C_3 symmetry (Fig. 2b), in strike comparison with the vacancy case. The atomic positions in the opposite layer are barely affected, and the band structure of the system shows a triple point crossing at the K point (Fig. 4a). In a spin polarized calculation, a spin splitting appears in the band structure, breaking time reversal symmetry as

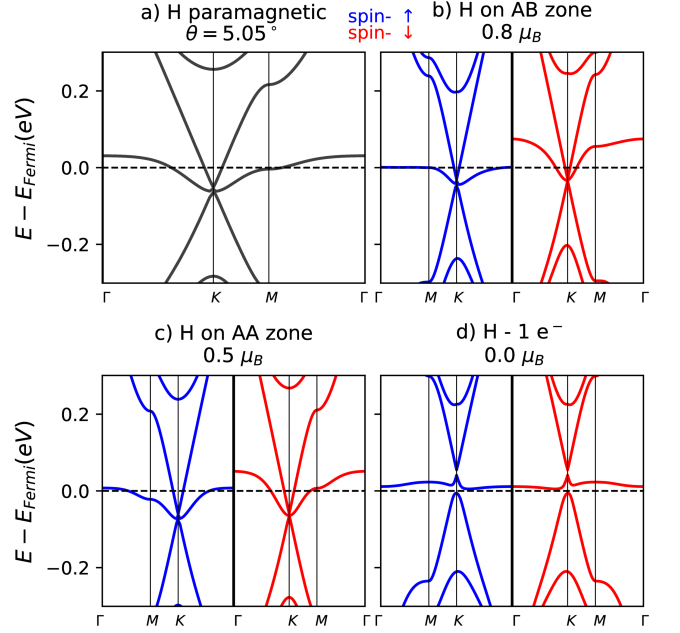


FIG. 4. a) First-principles paramagnetic band structure of mono-hydrogenated $\alpha \approx 5^\circ$ tBLG. When an H atom is attached to a C atom in the AB b) and AA c) regions, a local magnetic moment arises in the system, lifting the original spin degeneracy. Panels b) and c) show the unbalanced occupation of the nearly flat band in the up/down channels, yielding a local magnetic moment mentioned above. In this large angle regime $\alpha \approx 5^\circ$, removing one electron out of the system leads to a non-magnetic and gaped configuration, with an empty electronic flat-state in the vicinity of the Fermi level.

a consequence of the net magnetic moment triggered by the presence of the hydrogen zero mode (Fig. 4bc). In particular, the exchange field generates a shift of ~ 0.25 meV up and down of the impurity band. Interestingly, for any attachment position, the linear dispersion typical of graphene is preserved, although the Dirac cones are shifted in energy and a meV gap removes the Dirac point.

For an H atom sitting in the AB stacking region, one of the electronic bands associated with the defect is almost fully populated with one electron, whereas a similar band with opposite spin quantum number is almost empty. The total magnetic moment is of $0.8 \mu_B$. A similar behavior is observed for an H atom sitting on a AA stacked C atom, although the resulting magnetic moment decreases to $0.5 \mu_B$. A small n-type doping is induced in the layer opposite to the one with the H atom. This last feature can be inferred from the band diagrams of Fig. 4b and c, where the upper Dirac cone becomes slightly filled. This electron donor character demonstrates that both layers are partially hybridized through the defect state and a partial charge transfer occurs between layers. Finally, we consider the effect of a doping of a single electron per moiré supercell in this regime $\alpha \approx 5^\circ$. In that situation, we observe that the magnetic moment of the

impurity state is completely quenched (Fig.4d), yielding a fully occupied impurity band. As it will be shown in Sec. IV, the phenomenology at $\alpha \approx 1^\circ$ is dramatically different due to the appearance of the magic angle flat bands.

The previous phenomenology applies to twisted bilayers with large twisting angle $\alpha \approx 5^\circ$. In the following we will focus in smaller angles tBLG, that exhibit a substantially different behavior but for which DFT-based calculations are computationally demanding due to the large number of atoms in the unit cell. To circumvent such a limitation, the same phenomenology will be explored within a real-space tight-binding model, that allows to ultimately consider the effects of interactions in mono-hydrogenated magic angle superlattices with a more affordable computational cost and similar accuracy.

III. DEFECT-INDUCED STATES WITHIN A TIGHT-BINDING MODEL

We now move on to consider the effect of a single-H atom attached to the tBLG surface with an effective tight-binding model of the form

$$H_0 = \sum_{\langle ij \rangle} t c_i^\dagger c_j + \sum_{ij} t_\perp(\mathbf{r}_i, \mathbf{r}_j) c_i^\dagger c_j \quad (1)$$

where $\langle ij \rangle$ denotes sum over first neighbors in the same layer. The interlayer hopping $t_\perp(\mathbf{r})$ is modulated according to the structure of tBLG, which is taken as $t_\perp(\mathbf{r}_i, \mathbf{r}_j) = t_\perp \frac{(z_i - z_j)^2}{|\mathbf{r}_i - \mathbf{r}_j|^2} e^{-\beta(|\mathbf{r}_i - \mathbf{r}_j| - d)}$, with \mathbf{r}_i the position of site i and d the distance between layers. As a reference, the hopping parameters in graphene are $t \approx 3$ eV and $t_\perp \approx 0.4$ eV.⁶³ For computational convenience, in the tight-binding calculations an enhanced interlayer hopping is used, which allows us to recover the physics of small angle graphene superlattice with smaller units cells.^{64,65}

This low-energy tight-binding model aims to simplify the effect of removing a single p_z orbital by just eliminating a site out of the tBLG. As demonstrated in the DFT calculations above, this is equivalent to attaching a H atom to one of the bilayer surfaces. Furthermore, in the following we will be interested in the localization properties of the states in the moiré supercell. This can be easily computed within the tight-binding framework by means of the inverse participation ratio (IPR) of each Bloch wave function Ψ_n , that provides an estimation of the degree of localization of a state in a moiré unit cell: $IPR = \sum_i |\Psi_n(i)|^4$. For a fully extended state in the unit cell the IPR is a small value of $1/N$, where N is the number of atoms, whereas for a localized state it yields a large finite value even for large unit cells.

The emergence of magnetism is explored introducing a local Hubbard interaction term of the form

$$H_U = \sum_i U c_{i,\uparrow}^\dagger c_{i,\uparrow} c_{i,\downarrow}^\dagger c_{i,\downarrow} = \sum_i U n_{i,\uparrow} n_{i,\downarrow} \quad (2)$$

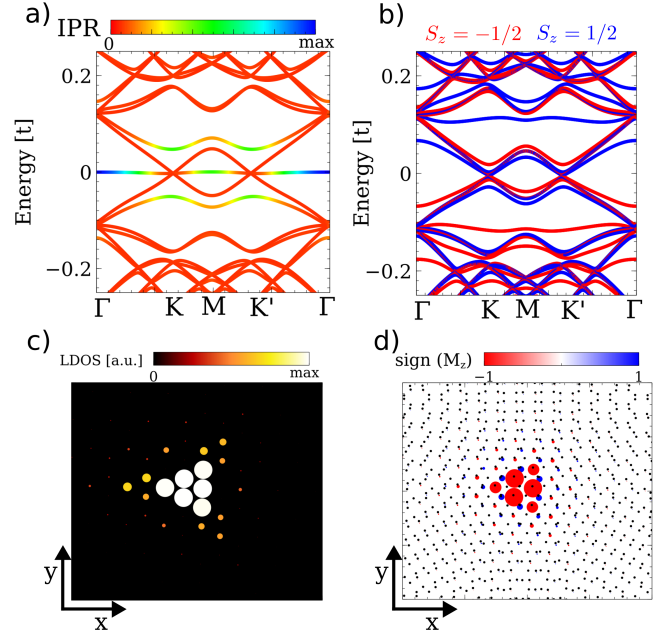


FIG. 5. a) Band structure of mono-hydrogenated tBLG with a twist angle $\alpha \approx 3^\circ$, showing the emergence of a flat band with a triple-point crossing. In b), the self-consistent band structure exhibits the emergence of an exchange splitting as a consequence of interactions. The real-space representation of the local density of states at Fermi level of panel a) is shown in c). The magnetism arising from the impurity state obtained after including interactions is shown in d).

where $n_{i,\uparrow} = c_{i,\uparrow}^\dagger c_{i,\uparrow}$ and $n_{i,\downarrow} = c_{i,\downarrow}^\dagger c_{i,\downarrow}$. The previous interaction is solved at the mean-field level $H_U \rightarrow H_U^{MF}$ with

$$H_U^{MF} = \sum_i U [\langle n_{i,\uparrow} \rangle n_{i,\downarrow} + \langle n_{i,\downarrow} \rangle n_{i,\uparrow} - \langle n_{i,\uparrow} \rangle \langle n_{i,\downarrow} \rangle] \quad (3)$$

We first address the case of a tBLG with a rotation angle of $\alpha \approx 3^\circ$, taking a single H atom per moiré unit cell (Fig. 5). Fig.5a shows that the paramagnetic band structure displays a flat band meeting the linearly dispersive bands, yielding a triple-point at the K and K' points. According to the color-resolved diagrams of the IPR (Fig. 5a), the nearly flat band at $E = 0$ is the most localized state in the supercell, which corresponds to the zero mode that build around the impurity (Fig. 5c). Including electronic interactions in the model leads to a spin-dependent band splitting (Fig.5b), with the consequent emergence of magnetism (Fig.5d). The real-space representation of the states associated to the flat band in Fig.5c demonstrates that they are the same that become magnetic (Fig. 5d). This results exemplify that the phenomenology of mono-hydrogenated tBLG obtained from the DFT calculations is captured by the low-energy tight-binding model.

We now move on to study the fate of the impurity bands as the magic angle regime is approached. In particular, at the magic angle regime, an additional set of

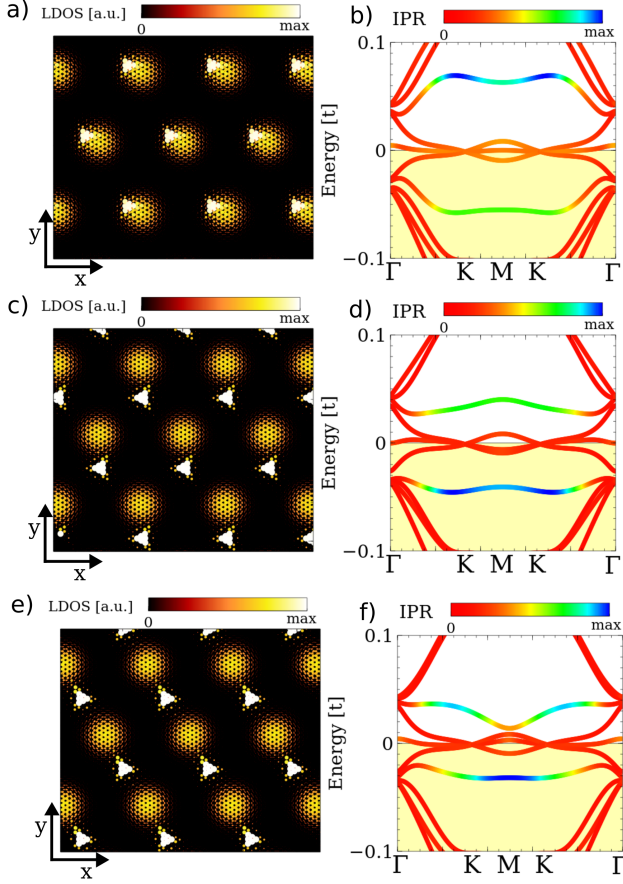


FIG. 6. Local density of states (a,c,e) and band structure (b,d,f) for tBLG with an H atom on the surface calculated with the low-energy tight binding model for $\alpha \approx 1.3^\circ$. In a) and b) the H atom is at the AA stacking region, in c) and d) in the AB region, and in e) and f) in the AB/BA interface. The color code of the band structures (b,d,f) reflects the localization of the state in the supercell. A triple-point crossing at the Fermi level is observed in all three cases.

bands is expected to appear, namely the flat AA bands¹⁰. In this situation, it is expected that the impurity band will heavily hybridize with the AA bands. To dive into this regime, a single H atom in a tBLG with twisting angle of $\alpha \approx 1.3^\circ$ (Fig. 6) is first considered. As shown in Fig. 6a), c), and e), a set of additional bands with highly reduced bandwidth appear close to the charge neutrality point. Again, a triple point is observed at the K and K' points in the band structure, for an impurity deposited on the AA region (Fig. 6ab), on the AB region (Fig. 6cd) and in the AB/BA boundary (Fig. 6ef). Interestingly, two additional bands appear close to charge neutrality point, having a substantially strong *IPR*. Those new bands appear due to the interplay of AA band with the impurity bands, that drifts spectral weight from the impurity state slightly above and below the charge neutrality point. Importantly, the small bandwidth of the AA bands suggests that the system may accommodate

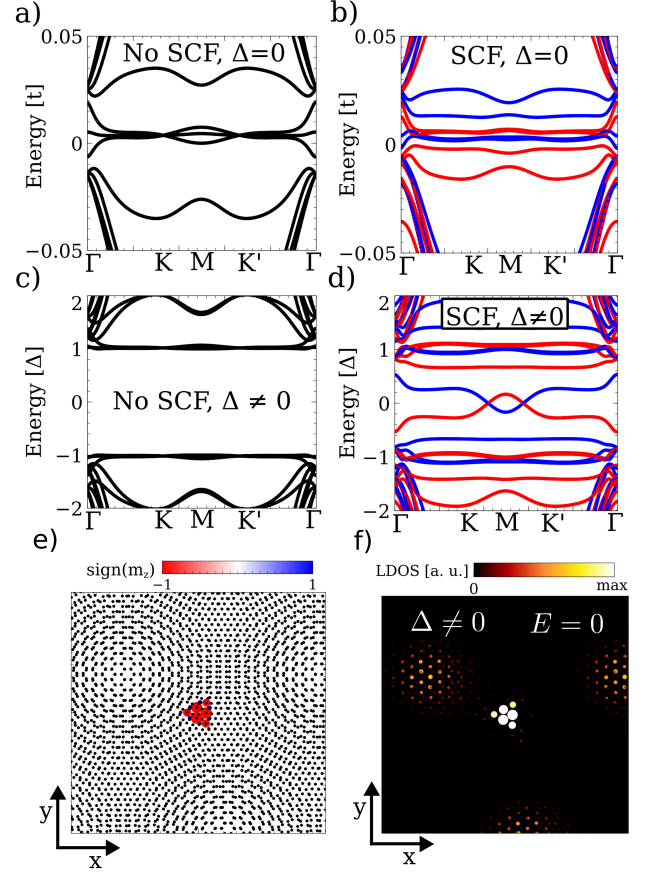


FIG. 7. a) Non-interacting band structure of a single vacancy in the AB region for a twist angle of $\alpha \approx 1^\circ$ and a doping of two holes with respect to charge neutrality. b) Exchange splitting arises when electronic interactions are included. In c) the non-interacting band structure opens a gap when a pairing Δ is included. d) shows the combined effect of the exchange interactions and superconductivity is the emergence of a band with energy smaller than Δ , signaling the emergence of Shiba-Rusinov states in the tBLG. Panel (e) shows the selfconsistent magnetization of (b) and (f) shows the local density of states of the in-gap bands of (d), highlighting that the in-gap Yu-Shiba-Rusinov state inherits the spatial distribution of the impurity induced magnetic moment. We took $U = 2t$ and $\Delta = 0.02t$.

extra electrons in the AA modes, instead of filling the impurity modes. This last feature becomes important in the next section when dealing with the interplay between magnetism and magic angle superconductivity.

IV. DEFECT-INDUCED YU-SHIBA-RUSINOV STATES IN TWISTED BILAYER GRAPHENE

As the twist between the two layers approaches a rotation angle of $\alpha \approx 1^\circ$, the density of states of pristine twisted bilayer graphene is largely enhanced, triggering an electronic instability when the system is doped with nearly 2 holes per unit cell.^{5,66,67} In the following, we will

explore the interplay between the vacancy induced magnetism presented above, and the superconducting state found in magic angle superlattices.^{5,66,67} To demonstrate that a magnetic defect has an impact on the tBLG superconducting properties^{5,66,67}, the low-energy spectrum of a magnetic symmetry-broken tBLG is now studied by taking the Hamiltonian

$$H = H_0 + H_U^{MF} + H_{SC} \quad (4)$$

where $H_{SC} = \sum_i \Delta_i [c_{i,\uparrow} c_{i,\downarrow} + c_{i,\downarrow}^\dagger c_{i,\uparrow}^\dagger]$. For the sake of concreteness, we take $\Delta_i = \Delta$, realizing a spatially uniform s-wave superconducting singlet pairing.^{68–71} We point out that additional superconducting symmetries have been proposed for magic angle superlattices besides the one consider above.^{18,19}

We first consider the case without superconducting order, namely $\Delta = 0$. The non-interacting band structure for an angle $\alpha \approx 1^\circ$ tBLG mono-hydrogenated in the AB region is shown in Fig.7a. The triple-point survives in this small angle regime and the flat band is strongly hybridized with the nearly flat Dirac cones, located in the AA region. In addition, new bands appear close to charge neutrality carry spectral weight of the impurity state. The fate of the impurity-induced magnetic state triggered by electron interactions is considered next. When introducing interactions and doping with two holes per moiré unit cell, the impurity induced magnetic moment survives (Fig.7b) and e)). This strikingly compares with the large angle scenario, in which doping with a single electron per moiré unit cell already destroys the impurity-induced magnetism.

We now unveil the effect of superconductivity in the previous setup. For that sake, a superconducting term is included on top of the normal state Hamiltonian. In a system with time-reversal symmetry and uniform pairing, the BdG eigenvalues ϵ_k are given by $\epsilon_k = \pm \sqrt{E_k^2 + \Delta^2}$, where E_k are the Bloch eigenvalues in the absence of superconductivity. Namely, the BdG band structure of a nonmagnetic system shows a gap of 2Δ in the spectra. This is observed in Fig.7c, where the superconducting field was included on top of the paramagnetic non-interacting band structure.

In the presence of magnetic moments, states inside the superconducting gap can appear due to the breaking of time reversal symmetry. In particular, Yu-Shiba-Rusinov states^{72–76} are in-gap modes in the superconducting spectrum that appear as a result of the time-reversal symmetry breaking introduced by local magnetic moments. Adding a uniform superconducting pairing Δ to the self-consistent solution of Fig.7b, two in-gap bands are observed in the BdG spectrum, as shown in Fig.7d. Interestingly, the Yu-Shiba-Rusinov state (Fig. 7f) reflects the spatial structure of the magnetic state (Fig. 7e).^{73–75} This results highlight that the impurity-induced magnetic moment of the tBLG can coexist with the superconducting state, generating in-gap Yu-Shiba-Rusinov states that could be observed by means of scanning tunnel microscope.^{73–75}

Finally, it is interesting to note that the energy of this Yu-Shiba-Rusinov states cannot be easily estimated as in conventional metals hosting magnetic impurities.⁷² In those instances, the energy of the in-gap state generated in the superconducting states takes the form^{72,77} $\epsilon = \Delta \frac{1-(JS\pi\rho/2)^2}{1+(JS\pi\rho/2)^2}$ where J is the exchange coupling between the impurity and the conduction electrons, S is the spin of the impurity, and ρ is the density of states in the normal state. In mono-hydrogenated tBLG the density of states in the normal state is divergent due to the existence of nearly flat bands, and the onset of magnetism changes substantially the density of states and the Fermi energy, invalidating the previous procedure. This phenomenology is also found in hydrogenated. monolayer graphene⁷⁸ Nevertheless, the emergence of Yu-Shiba-Rusinov states is a robust feature, as shown in the exact solution presented above.

V. CONCLUSIONS

To summarize, we have presented a detailed description of the impact of two types defects on the electronic and magnetic properties of twisted bilayer graphene. Localized states are found for both a vacancy and mono-hydrogenation of tBLG, which yield spatially localized magnetic states. Both types of defects remove effectively a p_z electron out of the bilayer. On one hand, mono-hydrogenation defect states modify the low-energy band diagram at the charge neutrality point creating a triple-point. On the other hand, a carbon vacancy yields impurity bands at different energies, distorting the π bands at the Fermi level. Interestingly, the presence of impurities leads to the emergence of spatially localized magnetic moments whose magnitude depends on the location of the defect.

In the magic angle regime, doping with two holes per moiré unit cell does not destroy the hydrogen induced magnetic moment, suggesting that such a defect-induced magnetism may coexist with the superconducting state. Including a superconducting term in the Hamiltonian, the interplay between defect-induced magnetism and superconductivity gives rise to in-gap Yu-Shiba-Rusinov states in the twisted bilayer. Our results demonstrate that atomic imperfections may have a substantial impact in the spectral properties of superconducting twisted graphene superlattices.

ACKNOWLEDGMENTS

Los Alamos National Laboratory is managed by Triad National Security, LLC, for the National Nuclear Security Administration of the U.S. Department of Energy under Contract No. 89233218CNA000001. This work was supported by the U.S. DOE Office of Basic Energy Sciences Program E3B5. We thank I. Brihuega, E. Cortes-del

Rio and A. Ramires for fruitful discussions. A.L.-B. acknowledges the computing resources provided on Bebop, the high-performance computing clusters operated by the Laboratory Computing Resource Center at Argonne National Laboratory. J. L. L. acknowledges financial support from the ETH Fellowship program.

APPENDIX

Appendix A: First-principles calculations

The description of the coupling between the graphitic layers before and after the introduction of an impurity was conducted through self-consistent calculations with the SIESTA code within a localized orbital basis set scheme. Spin-polarized calculations were conducted using a double- ζ basis set, and the local density approximation (LDA) approach for the exchange-correlation functional was used. Atomic positions of systems formed by over 508 atoms were fully relaxed with a force tolerance of 0.01 eV/Å. The integration over the Brillouin zone (BZ) was performed using a Monkhorst sampling of $7 \times 7 \times 1$ k-points. The radial extension of the orbitals had a finite range with a kinetic energy cutoff of 50 meV. A vertical separation of 25 Å in the simulation box prevents virtual periodic parallel layers from interacting.

-
- * alejandrolb@gmail.com
- ¹ A. H. Castro Neto, F. Guinea, N. M. R. Peres, K. S. Novoselov, and A. K. Geim, *Rev. Mod. Phys.* **81**, 109 (2009).
 - ² A. K. Geim and I. V. Grigorieva, *Nature* **499**, 419 (2013).
 - ³ J. M. B. Lopes dos Santos, N. M. R. Peres, and A. H. Castro Neto, *Phys. Rev. Lett.* **99**, 256802 (2007).
 - ⁴ P. Rickhaus, J. Wallbank, S. Slizovskiy, R. Pisoni, H. Overweg, Y. Lee, M. Eich, M.-H. Liu, K. Watanabe, T. Taniguchi, T. Ihn, and K. Ensslin, *Nano Letters* **18**, 6725 (2018).
 - ⁵ Y. Cao, V. Fatemi, S. Fang, K. Watanabe, T. Taniguchi, E. Kaxiras, and P. Jarillo-Herrero, *Nature* **556**, 43 (2018).
 - ⁶ Y. Cao, V. Fatemi, A. Demir, S. Fang, S. L. Tomarken, J. Y. Luo, J. D. Sanchez-Yamagishi, K. Watanabe, T. Taniguchi, E. Kaxiras, R. C. Ashoori, and P. Jarillo-Herrero, *Nature* **556**, 80 (2018).
 - ⁷ A. L. Sharpe, E. J. Fox, A. W. Barnard, J. Finney, K. Watanabe, T. Taniguchi, M. A. Kastner, and D. Goldhaber-Gordon, *arXiv e-prints*, arXiv:1901.03520 (2019), arXiv:1901.03520 [cond-mat.mes-hall].
 - ⁸ Y. Cao, D. Chowdhury, D. Rodan-Legrain, O. Rubies-Bigordà, K. Watanabe, T. Taniguchi, T. Senthil, and P. Jarillo-Herrero, *arXiv e-prints*, arXiv:1901.03710 (2019), arXiv:1901.03710 [cond-mat.str-el].
 - ⁹ Y. Jiang, J. Mao, X. Lai, K. Watanabe, T. Taniguchi, K. Haule, and E. Y. Andrei, *arXiv e-prints*, arXiv:1904.10153 (2019), arXiv:1904.10153 [cond-mat.mes-hall].
 - ¹⁰ E. Suárez Morell, J. D. Correa, P. Vargas, M. Pacheco, and Z. Barticevic, *Phys. Rev. B* **82**, 121407 (2010).
 - ¹¹ R. Bistritzer and A. H. MacDonald, *Proceedings of the National Academy of Sciences* **108**, 12233 (2011).
 - ¹² P. San-Jose and E. Prada, *Phys. Rev. B* **88**, 121408 (2013).
 - ¹³ A. Ramires and J. L. Lado, *Phys. Rev. Lett.* **121**, 146801 (2018).
 - ¹⁴ J. Kang and O. Vafek, *Phys. Rev. X* **8**, 031088 (2018).
 - ¹⁵ M. Koshino, N. F. Q. Yuan, T. Koretsune, M. Ochi, K. Kuroki, and L. Fu, *Phys. Rev. X* **8**, 031087 (2018).
 - ¹⁶ H. C. Po, L. Zou, A. Vishwanath, and T. Senthil, *Phys. Rev. X* **8**, 031089 (2018).
 - ¹⁷ F. Guinea and N. R. Walet, *Proceedings of the National Academy of Sciences* **115**, 13174 (2018).
 - ¹⁸ H. Isobe, N. F. Q. Yuan, and L. Fu, *Phys. Rev. X* **8**, 041041 (2018).
 - ¹⁹ C. Xu and L. Balents, *Phys. Rev. Lett.* **121**, 087001 (2018).
 - ²⁰ B. L. Chittari, N. Leconte, S. Javvaji, and J. Jung, *Electronic Structure* **1**, 015001 (2018).
 - ²¹ M. Yankowitz, S. Chen, H. Polshyn, Y. Zhang, K. Watanabe, T. Taniguchi, D. Graf, A. F. Young, and C. R. Dean, *Science* **363**, 1059 (2019).
 - ²² S. Carr, S. Fang, P. Jarillo-Herrero, and E. Kaxiras, *Phys. Rev. B* **98**, 085144 (2018).
 - ²³ I. Brihuega and F. Yndurain, *The Journal of Physical Chemistry B* **122**, 595 (2018).
 - ²⁴ A. Ramires and J. L. Lado, *arXiv e-prints*, arXiv:1902.05862 (2019), arXiv:1902.05862 [cond-mat.mes-hall].
 - ²⁵ M. M. Ugeda, I. Brihuega, F. Guinea, and J. M. Gómez-Rodríguez, *Phys. Rev. Lett.* **104**, 096804 (2010).
 - ²⁶ O. V. Yazyev, *Reports on Progress in Physics* **73**, 056501 (2010).
 - ²⁷ J. J. Palacios, J. Fernández-Rossier, and L. Brey, *Phys. Rev. B* **77**, 195428 (2008).
 - ²⁸ V. M. Pereira, J. M. B. Lopes dos Santos, and A. H. Castro Neto, *Phys. Rev. B* **77**, 115109 (2008).
 - ²⁹ O. V. Yazyev and L. Helm, *Phys. Rev. B* **75**, 125408 (2007).
 - ³⁰ H. Gonzalez-Herrero, J. M. Gomez-Rodriguez, P. Mallet, M. Moaied, J. J. Palacios, C. Salgado, M. M. Ugeda, J.-Y. Veuillen, F. Yndurain, and I. Brihuega, *Science* **352**, 437 (2016).
 - ³¹ N. A. García-Martínez, J. L. Lado, D. Jacob, and J. Fernández-Rossier, *Phys. Rev. B* **96**, 024403 (2017).
 - ³² A. Lopez-Bezanilla, F. Triozon, and S. Roche, *Nano Letters* **9**, 2537 (2009).

- ³³ J. M. Campanera, G. Savini, I. Suarez-Martinez, and M. I. Heggie, *Phys. Rev. B* **75**, 235449 (2007).
- ³⁴ S. Dai, Y. Xiang, and D. J. Srolovitz, *Nano Letters* **16**, 5923 (2016), pMID: 27533089, <https://doi.org/10.1021/acs.nanolett.6b02870>.
- ³⁵ S. Latil and L. Henrard, *Phys. Rev. Lett.* **97**, 036803 (2006).
- ³⁶ S. Latil, V. Meunier, and L. Henrard, *Phys. Rev. B* **76**, 201402 (2007).
- ³⁷ F. Gargiulo, G. Autès, N. Virk, S. Barthel, M. Rösner, L. R. M. Toller, T. O. Wehling, and O. V. Yazyev, *Phys. Rev. Lett.* **113**, 246601 (2014).
- ³⁸ J. Katoch, T. Zhu, D. Kochan, S. Singh, J. Fabian, and R. K. Kawakami, *Phys. Rev. Lett.* **121**, 136801 (2018).
- ³⁹ D. Soriano, N. Leconte, P. Ordejón, J.-C. Charlier, J.-J. Palacios, and S. Roche, *Phys. Rev. Lett.* **107**, 016602 (2011).
- ⁴⁰ M. Gmitra, D. Kochan, and J. Fabian, *Phys. Rev. Lett.* **110**, 246602 (2013).
- ⁴¹ M. V. Ulybyshev and M. I. Katsnelson, *Phys. Rev. Lett.* **114**, 246801 (2015).
- ⁴² D. Kochan, M. Gmitra, and J. Fabian, *Phys. Rev. Lett.* **112**, 116602 (2014).
- ⁴³ D. Wong, Y. Wang, W. Jin, H.-Z. Tsai, A. Bostwick, E. Rotenberg, R. K. Kawakami, A. Zettl, A. A. Mostofi, J. Lischner, and M. F. Crommie, *Phys. Rev. B* **98**, 155436 (2018).
- ⁴⁴ M. Farjam, D. Haberer, and A. Grüneis, *Phys. Rev. B* **83**, 193411 (2011).
- ⁴⁵ B. R. Matis, B. H. Houston, and J. W. Baldwin, *Phys. Rev. B* **88**, 085441 (2013).
- ⁴⁶ J. A. Vergés and P. L. de Andres, *Phys. Rev. B* **81**, 075423 (2010).
- ⁴⁷ Y. Lei, S. A. Shevlin, W. Zhu, and Z. X. Guo, *Phys. Rev. B* **77**, 134114 (2008).
- ⁴⁸ E. H. Lieb, *Phys. Rev. Lett.* **62**, 1201 (1989).
- ⁴⁹ O. V. Yazyev, *Phys. Rev. Lett.* **101**, 037203 (2008).
- ⁵⁰ Y. Zhang, S.-Y. Li, H. Huang, W.-T. Li, J.-B. Qiao, W.-X. Wang, L.-J. Yin, K.-K. Bai, W. Duan, and L. He, *Phys. Rev. Lett.* **117**, 166801 (2016).
- ⁵¹ P. O. Lehtinen, A. S. Foster, Y. Ma, A. V. Krashennnikov, and R. M. Nieminen, *Phys. Rev. Lett.* **93**, 187202 (2004).
- ⁵² J. O. Sofo, G. Usaj, P. S. Cornaglia, A. M. Suarez, A. D. Hernández-Nieves, and C. A. Balseiro, *Phys. Rev. B* **85**, 115405 (2012).
- ⁵³ E. Nakhmedov, E. Nadimi, S. Vedaei, O. Alekperov, F. Tatardar, A. I. Najafov, I. I. Abbasov, and A. M. Saletsky, *Phys. Rev. B* **99**, 125125 (2019).
- ⁵⁴ V. G. Miranda, L. G. G. V. Dias da Silva, and C. H. Lewenkopf, *Phys. Rev. B* **94**, 075114 (2016).
- ⁵⁵ B. Wang and S. T. Pantelides, *Phys. Rev. B* **86**, 165438 (2012).
- ⁵⁶ R. E. Mapasha, A. M. Ukpog, and N. Chetty, *Phys. Rev. B* **85**, 205402 (2012).
- ⁵⁷ S. Yuan, H. De Raedt, and M. I. Katsnelson, *Phys. Rev. B* **82**, 235409 (2010).
- ⁵⁸ A. Ferreira, J. Viana-Gomes, J. Nilsson, E. R. Mucciolo, N. M. R. Peres, and A. H. Castro Neto, *Phys. Rev. B* **83**, 165402 (2011).
- ⁵⁹ H. P. Dahal, A. V. Balatsky, and J.-X. Zhu, *Phys. Rev. B* **77**, 115114 (2008).
- ⁶⁰ J. J. Palacios and F. Ynduráin, *Phys. Rev. B* **85**, 245443 (2012).
- ⁶¹ M. Andelkovic, L. Covaci, and F. M. Peeters, *Phys. Rev. Materials* **2**, 034004 (2018).
- ⁶² K. Ulman and S. Narasimhan, *Phys. Rev. B* **89**, 245429 (2014).
- ⁶³ A. O. Sboychakov, A. L. Rakhmanov, A. V. Rozhkov, and F. Nori, *Phys. Rev. B* **92**, 075402 (2015).
- ⁶⁴ M.-H. Liu, P. Rickhaus, P. Makk, E. Tóvári, R. Maurand, F. Tkatschenko, M. Weiss, C. Schönenberger, and K. Richter, *Phys. Rev. Lett.* **114**, 036601 (2015).
- ⁶⁵ S. Carr, S. Fang, P. Jarillo-Herrero, and E. Kaxiras, *Phys. Rev. B* **98**, 085144 (2018).
- ⁶⁶ X. Lu, P. Stepanov, W. Yang, M. Xie, M. A. Aamir, I. Das, C. Urgell, K. Watanabe, T. Taniguchi, G. Zhang, A. Bachtold, A. H. MacDonald, and D. K. Efetov, *arXiv e-prints*, arXiv:1903.06513 (2019), arXiv:1903.06513 [cond-mat.str-el].
- ⁶⁷ M. Yankowitz, S. Chen, H. Polshyn, Y. Zhang, K. Watanabe, T. Taniguchi, D. Graf, A. F. Young, and C. R. Dean, *Science* (2019), 10.1126/science.aav1910.
- ⁶⁸ F. Wu, A. H. MacDonald, and I. Martin, *Phys. Rev. Lett.* **121**, 257001 (2018).
- ⁶⁹ Y. W. Choi and H. J. Choi, *Phys. Rev. B* **98**, 241412 (2018).
- ⁷⁰ H. Polshyn, M. Yankowitz, S. Chen, Y. Zhang, K. Watanabe, T. Taniguchi, C. R. Dean, and A. F. Young, *arXiv e-prints*, arXiv:1902.00763 (2019), arXiv:1902.00763 [cond-mat.str-el].
- ⁷¹ B. Lian, Z. Wang, and B. A. Bernevig, *arXiv e-prints*, arXiv:1807.04382 (2018), arXiv:1807.04382 [cond-mat.mes-hall].
- ⁷² A. V. Balatsky, I. Vekhter, and J.-X. Zhu, *Rev. Mod. Phys.* **78**, 373 (2006).
- ⁷³ M. Ruby, Y. Peng, F. von Oppen, B. W. Heinrich, and K. J. Franke, *Phys. Rev. Lett.* **117**, 186801 (2016).
- ⁷⁴ M. Ruby, B. W. Heinrich, Y. Peng, F. von Oppen, and K. J. Franke, *Phys. Rev. Lett.* **120**, 156803 (2018).
- ⁷⁵ M. Ruby, F. Pientka, Y. Peng, F. von Oppen, B. W. Heinrich, and K. J. Franke, *Phys. Rev. Lett.* **115**, 087001 (2015).
- ⁷⁶ T. O. Wehling, H. P. Dahal, A. I. Lichtenstein, and A. V. Balatsky, *Phys. Rev. B* **78**, 035414 (2008).
- ⁷⁷ H. Shiba, *Progress of Theoretical Physics* **40**, 435 (1968).
- ⁷⁸ J. L. Lado and J. Fernández-Rossier, *2D Materials* **3**, 025001 (2016).